Annual Review of Marine Science

The Global Overturning Circulation

Paola Cessi

Scripps Institution of Oceanography, University of California, San Diego, La Jolla, California 92093-0213, USA; email: pcessi@ucsd.edu

Annu. Rev. Mar. Sci. 2019. 11:249–70

The *Annual Review of Marine Science* is online at marine.annualreviews.org

https://doi.org/10.1146/annurev-marine-010318-095241

Keywords

meridional overturning circulation, ocean dynamics

Abstract

In this article, I use the Estimating the Circulation and Climate of the Ocean version 4 (ECCO4) reanalysis to estimate the residual meridional overturning circulation, zonally averaged, over the separate Atlantic and Indo-Pacific sectors. The abyssal component of this estimate differs quantitatively from previously published estimates that use comparable observations, indicating that this component is still undersampled. I also review recent conceptual models of the oceanic meridional overturning circulation and of the mid-depth and abyssal stratification. These theories show that dynamics in the Antarctic circumpolar region are essential in determining the deep and abyssal stratification. In addition, they show that a mid-depth cell consistent with observational estimates is powered by the wind stress in the Antarctic circumpolar region, while the abyssal cell relies on interior diapycnal mixing, which is bottom intensified.

1. ESTIMATES FROM OBSERVATIONS

Although the ocean is differentially heated and freshened almost exclusively very close to the surface (the exception being the small contribution provided by geothermal heating), the existence of temperature and salinity gradients throughout the water column implies flows that communicate downward the surface values. The mechanism for transferring buoyancy (and other tracers) in the upper ocean, i.e., the top few hundred meters, is well understood: The surface wind stress generates a shallow Ekman transport, the convergence of which in the subtropics pushes tracers down to a depth proportional to (the square root of) the wind-stress curl integrated over the longitudinal width of the basin, and inversely proportional to (the square root of) the local surface buoyancy gradient (Welander 1971). This is the main thermocline, bounding from below the double-well-shaped isopycnals in the upper levels of **Figure 1** (approximately above the upper horizontal dashed line).

Figure 1 shows that the densities higher than those in the main thermocline have steep slopes in the Antarctic Circumpolar Current (ACC) region, while north of the circumpolar latitudes (i.e., north of approximately 45°S), the slopes of the density surfaces in the mid-depth and abyssal regions are small in both basins (south of approximately 55°N).[1] However, an important asymmetry differentiates the Atlantic from the Pacific: The mid-depth density surfaces (i.e., those with σ_2 between 36 kg/m^3 and 37.52 kg/m^3 in **Figure 1*a***) steepen again and outcrop (i.e., reach the sea surface) in the northernmost latitudes of the Atlantic but not in the Pacific. The North Atlantic outcrop of the isopycnals with σ_2 between 36 kg/m^3 and 37.52 kg/m^3 marks the transformation of intermediate and thermocline waters into North Atlantic Deep Water (NADW), the water mass characterizing the southward branch of the clockwise mid-depth cell of the meridional overturning

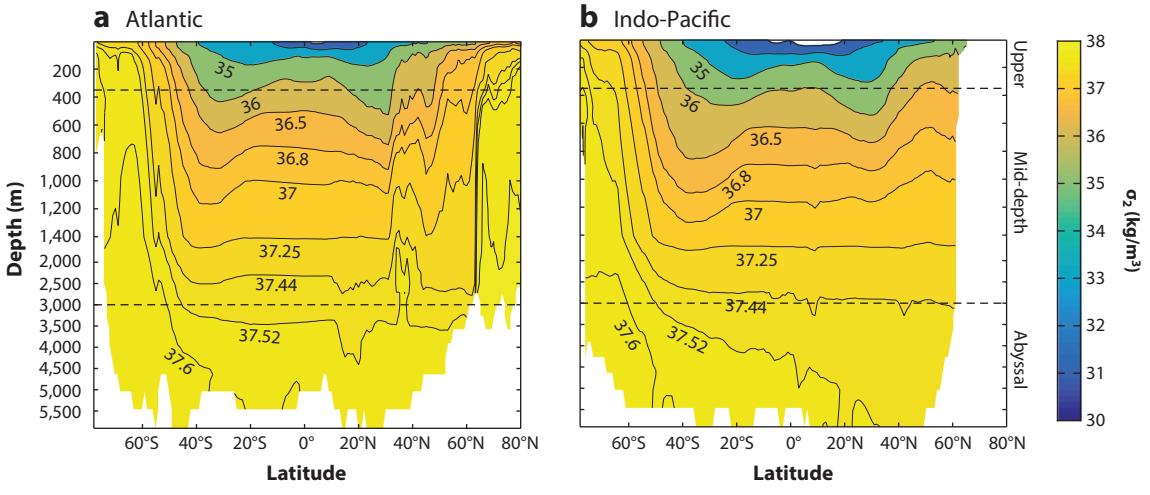

Figure 1

Potential density referenced to 2,100 dbar (σ_2) zonally averaged in (*a*) the Atlantic sector and (*b*) the Indo-Pacific sector from the Estimating the Circulation and Climate of the Ocean version 4 (ECCO4) reanalysis, showing the stratification as a function of latitude (abscissa) and depth (ordinate). Notice that the contour interval decreases with depth. The horizontal black dashed lines define the approximate boundaries between the upper, mid-depth, and abyssal regions. The white region indicates the maximum depth of the bottom.

Erratum >

[1] The localized isopycnal doming at 35°N in **Figure 1*a*** is due to the Mediterranean Sea, which is included in the zonal average of **Figure 1**.

circulation in the Atlantic sector (see **Figure 2*a***). There is no equivalent deep-water formation in the Pacific; Section 5 summarizes the reasons for this fundamental asymmetry. Conversely, the abyssal isopycnals (i.e., those with σ_2 below 37.52 kg/m^3 in **Figure 1*b***) slope downward and strike the bottom (incrop) in the North Pacific, marking the northward transport by the lower branch of the counterclockwise abyssal cell, a feature more prominent in the Indo-Pacific than in the

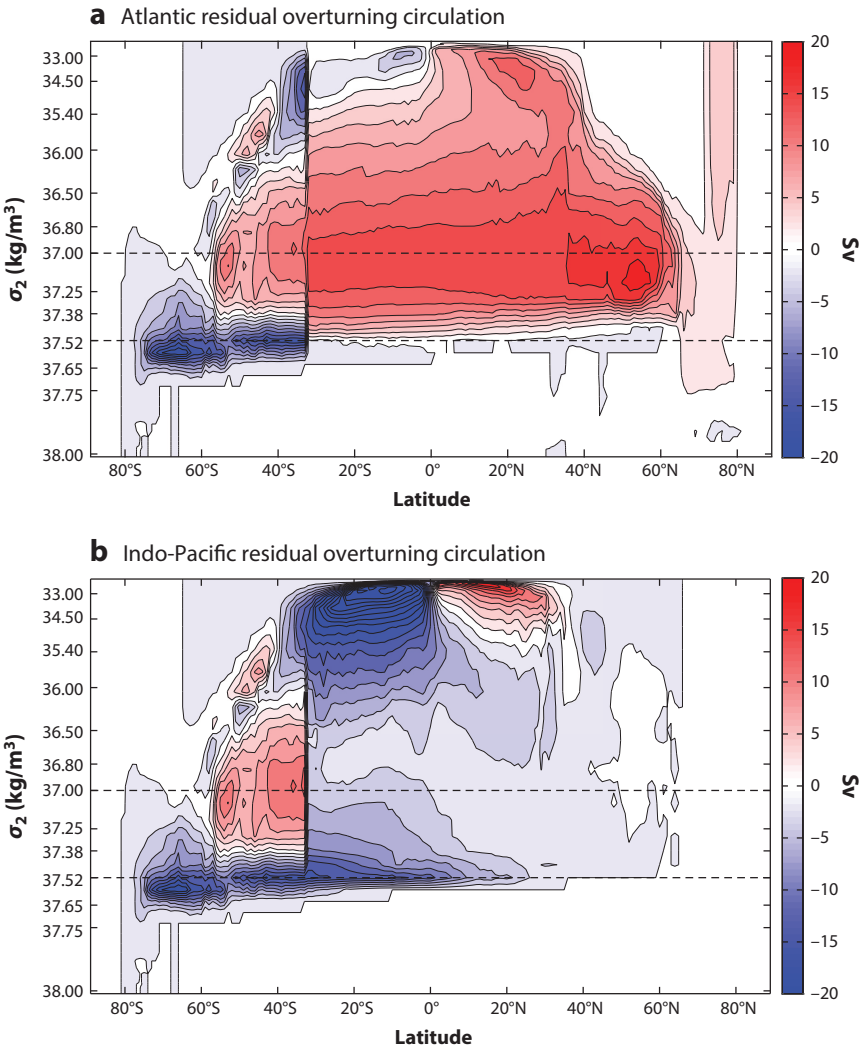

Figure 2

Meridional overturning circulation obtained by vertically integrating the meridional Eulerian velocity plus bolus velocity from the bottom to different surfaces of constant σ_2, then time averaging and zonally integrating over the Southern Ocean south of 33°S (both panels), over the Atlantic sector north of 33°S (panel *a*), and over the Indo-Pacific sector north of 33°S (panel *b*) from the Estimating the Circulation and Climate of the Ocean version 4 (ECCO4) reanalysis as a function of latitude (abscissa) and σ_2 (ordinate). The red clockwise cell in panel *a* is the mid-depth cell, and the blue counterclockwise cell below $\sigma_2 = 37$ kg/m^3 in panel *b* is the abyssal cell. The contour interval is 2 Sv. The horizontal dashed lines mark $\sigma_2 = 37$ kg/m^3 and $\sigma_2 = 37.52$ kg/m^3.

Atlantic (see **Figure 2*b***). This cell is fed by the formation of Antarctic Bottom Water (AABW) at the highest latitudes of the Antarctic region and is balanced by diapycnal upwelling in the interior. The larger range of incropping surfaces in the Indo-Pacific compared with the Atlantic is relevant because, as discussed in Section 4, it shows that a larger volume of water is in contact with rough topography and ridges in the Indo-Pacific than in the Atlantic. Consistently, bottom roughness is maximum in the East Pacific (see figure 1 of Whalen et al. 2015).

The flows that transport tracers in the mid-depth and abyssal regions are part of a global overturning circulation formed by two main interconnected cells: a mid-depth clockwise cell, confined to the Atlantic sector [called the Atlantic meridional overturning circulation (AMOC)], and an abyssal counterclockwise cell, most prominent in the Indo-Pacific sector (see **Figure 2**). Kuhlbrodt et al. (2007) published an extensive review of the AMOC. The main feature of the AMOC is that upper-ocean water (i.e., the thermocline and intermediate water) enters the Atlantic (defined in practice as the semienclosed region north of 30°S, including the Arctic, and bounded to the west by the American continent and Greenland and to the east by Europe and Africa) and proceeds northward and downward until it surfaces again in the Labrador and Nordic Seas, where it is densified and sinks, forming NADW. NADW flows southward in the Atlantic and surfaces in the Southern Ocean, where a portion is made less dense by surface freshening and heating and transformed into intermediate water, partially closing the loop of the mid-depth cell. The remaining portion of upwelled NADW is densified by cooling and brine rejection, which transform it into AABW and Circumpolar Deep Water. AABW and Circumpolar Deep Water sink near the Antarctic continent to the abyssal regions, where they flow northward, forming the abyssal cell (Lumpkin & Speer 2007). The portion of NADW transformed into AABW and Circumpolar Deep Water is eventually further transformed by abyssal mixing to water lighter than approximately $\sigma_2 = 37.25$ kg/m^3. Above this value, water can be brought up to the surface (mostly along isopycnals) by the strong Ekman suction of the Southern Hemisphere subpolar region, where it is transformed into intermediate water by surface freshening and heating, closing the remaining part of the mid-depth cell (Marshall & Speer 2012).

The transport of the mid-depth and abyssal cells is quantified in **Figure 2**, which shows the meridional velocity, vertically integrated from the bottom to 50 different levels of constant potential density (σ_2), and then integrated in longitude and averaged in time as a function of σ_2 and latitude. The meridional velocity is obtained from the Estimating the Circulation and Climate of the Ocean version 4 (ECCO4) reanalysis, which assimilates many observations into a primitive-equation ocean/sea-ice model (Forget et al. 2015). The meridional velocity used in **Figure 2** is the sum of the Eulerian velocity plus the bolus velocity. The bolus velocity represents the transport of water effected by mesoscale eddies, which are not resolved by the ECCO4 grid but are parameterized in terms of resolved quantities (Gent & McWilliams 1990, Griffies 1998). The motivation for integrating the Eulerian velocity plus the bolus velocity below potential-density surfaces is that the resulting overturning, called the residual overturning circulation, quantifies the transport across isopycnals—i.e., the transformation among different density classes due to surface heat and freshwater fluxes, interior diapycnal mixing, and bottom geothermal heating. The residual overturning circulation is considered to be more representative of the transport of tracers than the transport obtained by integrating the meridional velocity from the bottom to fixed depth levels (Andrews et al. 1987, Young 2012).

In this analysis of the ECCO4 estimate, the AMOC peaks at 19 sverdrups (Sv; 1 Sv = 10^6 m^3/s), and the cross-equatorial transport is 15 Sv, in line with previous estimates from the analysis of hydrographic data (Lumpkin & Speer 2007, Talley 2013) and from moored measurements at 34.5°S (Meinen et al. 2018) and at 26.5°N (McCarthy et al. 2015). **Table 1** summarizes these recent estimates of the Atlantic mid-depth transports.

Table 1 Summary of transport estimates of the Atlantic mid-depth cell

Estimate	Data	Transport at 30°S (Sv)	Maximum transport (Sv)
ECCO4	Hydrography, Argo, sea-surface temperature, altimeter, geoid, MITgcm	15	19
Lumpkin & Speer 2007	Hydrography, inverse	12	18
Talley 2013	Hydrography	13	18
Meinen et al. 2018	Moored density profiles, bottom pressure, satellite winds	15 (at 34.5°S)	NA
McCarthy et al. 2015	Moored density profiles, bottom cable, satellite winds	NA	17 (at 26.5°N)

Abbreviations: ECCO4, Estimating the Circulation and Climate of the Ocean version 4; MITgcm, MIT General Circulation Model; NA, not applicable.

In the ECCO4 estimate, both the northward and the southward branches of the AMOC flow along surfaces of constant σ_2, except for the NADW formation region and the circumpolar region, showing that very little diapycnal transformation occurs throughout most of the Atlantic basin at these depths.

The abyssal cell in ECCO4 peaks at 15 Sv north of 30°S (20 Sv south of 30°S), a value on the low side of recent observational estimates based on analyses of hydrographic data: Lumpkin & Speer (2007) estimated 21±7 Sv, while Talley (2013) estimated 29 Sv. Kunze (2017) and de Lavergne et al. (2016a,b) determined the transport of the abyssal cell by estimating the diapycnal mixing that supports the return of the upward and northward branch of the abyssal overturning. This approach calculates the diapycnal velocity and infers the resulting along-isopycnal meridional transport, while the traditional approach based on hydrography calculates the meridional transport along isopycnals and infers the diapycnal component. Kunze (2017) estimated that the abyssal cell peaks at 20 Sv; the diapycnal mixing was calculated from an estimate of internal-wave strain that uses concurrent velocity, temperature, salinity, and depth profiles (Kunze et al. 2006), combined with a parameterization relating strain to mixing (Henyey et al. 1986). De Lavergne et al. (2016b) estimated 10–15 Sv of abyssal water upwelling north of 30°S, using estimates of geothermal heating and internal- and lee-wave dissipation near the ocean bottom, together with a parameterization relating energy dissipation to diapycnal mixing (Bouffard & Boegman 2013). The range of estimates by de Lavergne et al. (2016b) reflects the range of choices in the parameterization of mixing. **Table 2** summarizes the transport estimates for the abyssal cell, showing a larger uncertainty for the abyssal cell than for the mid-depth cell (cf. **Table 1**).

Table 2 Summary of transport estimates of the global abyssal cell

Estimate	Data	Transport at 30°S (Sv)	Maximum transport (Sv)
ECCO4	Hydrography, Argo, sea-surface temperature, altimeter, geoid, MITgcm	15	20
Lumpkin & Speer 2007	Hydrography, inverse	21	21
Talley 2013	Hydrography	29	29
Kunze 2017	Diapycnal mixing from strain measurements	NA	20
De Lavergne et al. 2016b	Diapycnal mixing from internal wave dissipation	NA	10–15

Abbreviations: ECCO4, Estimating the Circulation and Climate of the Ocean version 4; MITgcm, MIT General Circulation Model; NA, not applicable.

It is remarkable that the transport of both the mid-depth and abyssal cells is comparable to the transport of the subtropical cells in the upper ocean, associated with the local surface Ekman transport and the subtropical gyres. The subtropical cells can be seen above $\sigma_2 = 36.0$ kg/m^3 in **Figure 2*a*** and above $\sigma_2 = 36.8$ kg/m^3 in **Figure 2*b***. The larger depth and density range of the subtropical cell in the Southern Hemisphere of the Indo-Pacific relative to the Atlantic is due to the large longitudinal extent of the Indo-Pacific basin, which occupies approximately 270° of longitude in the Southern Hemisphere, spanning from the east coast of Africa to the west coast of South America. Additionally, the maximum amplitude of westerly wind stress in the Southern Hemisphere is almost three times the westerly wind stress in the Northern Hemisphere, leading to a wide and strong supergyre that penetrates much farther down in the water column than its Northern Hemisphere counterparts (Ridgway & Dunn 2007, Speich et al. 2007).

The mid-depth and abyssal transports are distributed over a larger range of depth than the subtropical cells: The AMOC and the abyssal cell each occupy approximately 2,000 m of depth, while the subtropical cells reach down to approximately 500 m in the Atlantic and approximately 1,200 m in the Indo-Pacific. Therefore, the velocities are proportionally smaller in the mid-depth and abyssal cells relative to the subtropical cells.

The zonally averaged meridional/vertical transports shown in **Figure 2** do not visualize well the three-dimensional pathways of the mid-depth and abyssal circulation; zonally averaging obscures the lateral exchanges occurring between the Southern Ocean and the basin sectors. These exchanges are difficult to quantify because particles in the Southern Ocean make many circumpolar circuits around Antarctica before entering a basin, sinking, or upwelling; the east–west recirculating transport of the ACC is more than an order of magnitude larger than the net exchange in or out of the various sectors of the circumpolar region.

There is agreement that approximately 18 Sv of NADW must be returned to intermediate and thermocline waters. But the details of this upward return from the lower branch of the AMOC to the upper branch differ among authors (Lumpkin & Speer 2007, Marshall & Speer 2012, Talley 2013). According to Lumpkin & Speer (2007) and Marshall & Speer (2012), 7 Sv of these 18 Sv follow a direct adiabatic route in the Southern Ocean to the surface mixed layer, where they are transformed into intermediate water by buoyancy gain; the other 11 Sv are recycled through the abyssal cell. The first step of recycling is densification into AABW by surface buoyancy loss, again in the Southern Ocean; the second step is descent via the downwelling branch of the abyssal cell, also in the Southern Ocean; and the third step is diapycnal upwelling, predominantly in the interior of the Indo-Pacific basin.

Talley (2013) argued instead that all 18 Sv of NADW are recycled through the abyssal cell. This view requires a greater amount of Indo-Pacific diapycnal mixing than does that of Lumpkin & Speer (2007) and Marshall & Speer (2012). Enhanced diapycnal mixing is found below the level of rough topographic features (St. Laurent et al. 2002, Nikurashin & Ferrari 2013, Waterhouse et al. 2014). The topographically enhanced mixing is effective 1,000–1,500 m above rough topography and ridges; above this depth, there is little mixing, and the flow is largely adiabatic, proceeding along isopycnals.

Both the adiabatic route and the abyssal recycling route involve adiabatic upwelling along isopycnals to transport deep water to the surface, where the local northward Ekman transport moves water back to the North Atlantic.

To highlight the challenges in determining the route for the return of NADW, **Figure 3** shows a view of the mass budget in ECCO4. Horizontally, the domain is divided into six regions: the Atlantic, Indian, and Pacific basins north of 30°S and the Atlantic, Indian, and Pacific sectors south of 30°S. Vertically, the domain is divided into three layers. **Figure 3** shows the mass budget above the potential-density surface $\sigma_2 = 37$ kg/m^3; this is the layer that contains the upper, northward

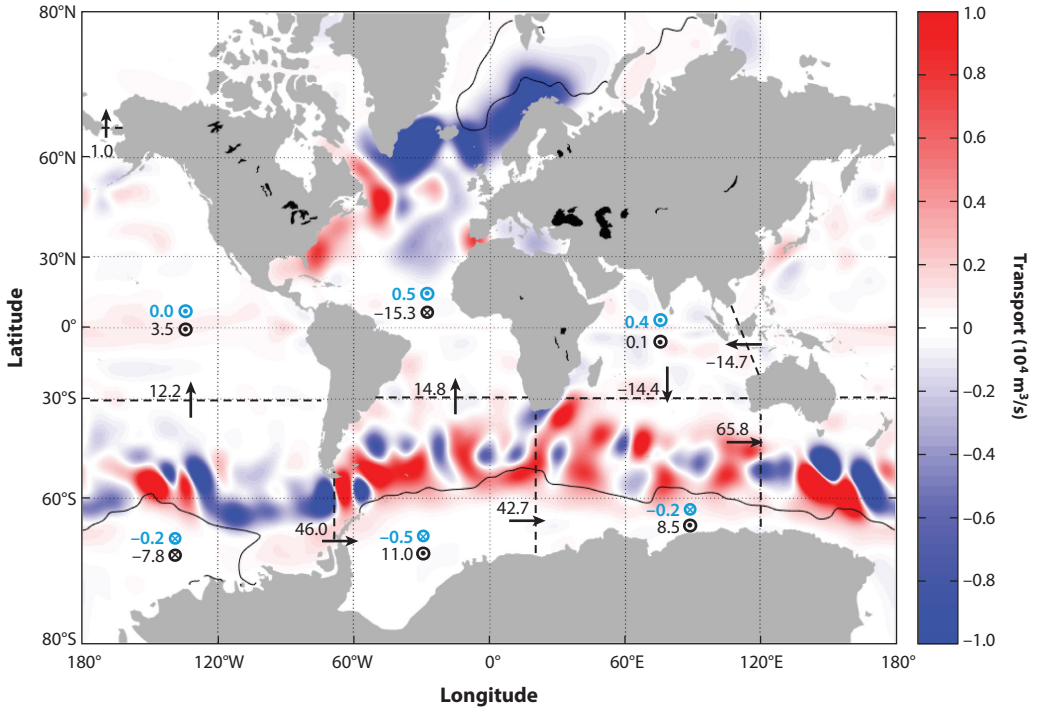

Figure 3

Smoothed diapycnal transport across the $\sigma_2 = 37$ kg/m^3 isopycnal (*colors*), showing section transports integrated vertically between $\sigma_2 = 37$ kg/m^3 and the sea surface (*black numerals with arrows*). Also shown are the net diapycnal transports horizontally integrated over the six sectors (*numerals with circles*), with black numerals indicating net transports across the $\sigma_2 = 37$ kg/m^3 isopycnal and blue numerals indicating net transports across the sea surface. The dotted circles indicate upwelling, and the crossed circles indicate downwelling. The black contour shows the climatological outcrop of the $\sigma_2 = 37$ kg/m^3 isopycnal.

branch of the mid-depth cell, i.e., the intermediate and thermocline waters. **Figure 4** shows the mass budget for 37 kg/m^3 $< \sigma_2 <$ 37.52 kg/m^3; this is the layer that contains the lower, southward branch of the mid-depth overturning, i.e., NADW. **Figure 5** shows the mass budget for the bottom layer, which contains the majority of the northward branch of the abyssal cell. The colored contours in **Figures 3–5** show the time-averaged diapycnal velocity across the isopycnals dividing the layers, i.e., across $\sigma_2 = 37$ kg/m^3 in **Figure 3** and across $\sigma_2 = 37.52$ kg/m^3 in **Figures 4** and **5**.

Despite the smoothing over four grid points in each direction, the diapycnal velocity is very spatially heterogeneous. Across $\sigma_2 = 37$ kg/m^3 (see **Figure 3**), diapycnal transformations are largely confined to the northern North Atlantic. The formation of NADW appears as the strong downwelling near the climatological outcrop (marked by a black contour in **Figure 3**). The upwelling near the western boundary of the North Atlantic accounts for the increase of the mid-depth cell transport from approximately 15 Sv across the equator to approximately 19 Sv at the NADW formation latitude. The other basins show little diapycnal transformation. In the Southern Ocean (i.e., south of 30°S), strong transformations occur at all longitudes, with a complex pattern of diapycnal downwelling and upwelling. The net transformation south of 30°S is from dense to light in the Atlantic (11 Sv) and Indian sectors (8.5 Sv) and from light to dense in the Pacific sector (−7.8 Sv).

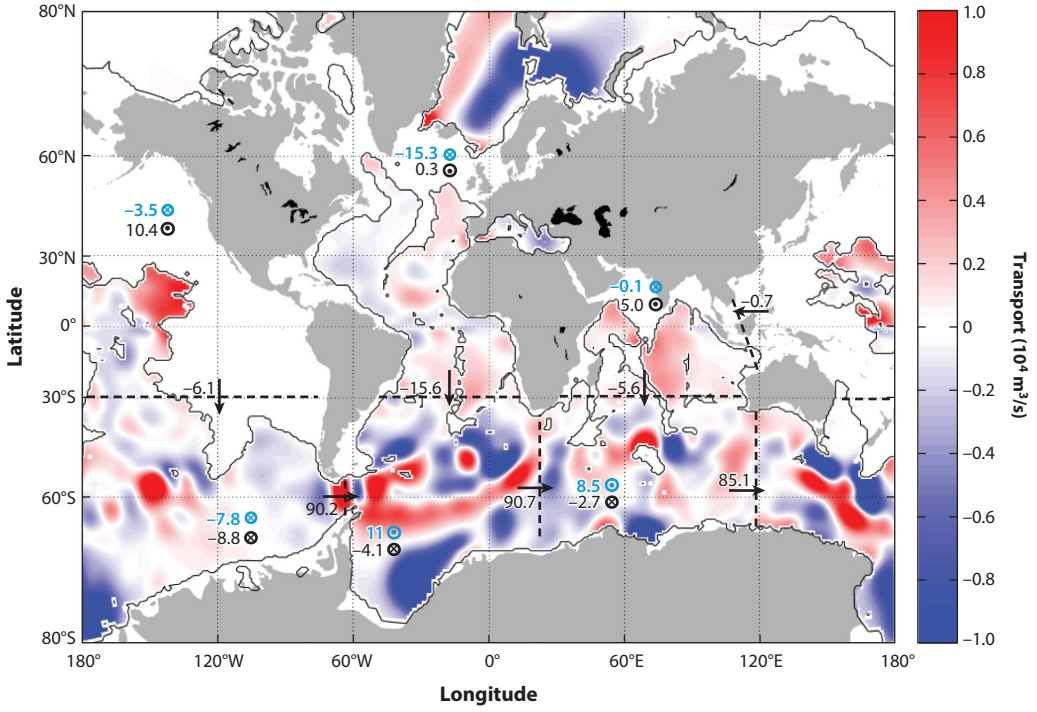

Figure 4

Smoothed diapycnal transport across the $\sigma_2 = 37.52$ kg/m^3 isopycnal (*colors*), showing section transports integrated vertically between $\sigma_2 = 37.52$ kg/m^3 and $\sigma_2 = 37$ kg/m^3 (*black numerals with arrows*). Also shown are the net diapycnal transports horizontally integrated over the six sectors (*numerals with circles*), with black numerals indicating net transports across the $\sigma_2 = 37.52$ kg/m^3 isopycnal and blue numerals indicating net transports across the $\sigma_2 = 37$ kg/m^3 isopycnal. The dotted circles indicate upwelling, and the crossed circles indicate downwelling. The black contour shows the climatological intersection at the bottom (incrop) of the $\sigma_2 = 37.52$ isopycnal.

Across $\sigma_2 = 37.52$ kg/m^3, diapycnal transformations are evident in the interior of the basins as well as in the northern North Atlantic and Southern Ocean. At this density, net upwelling occurs in all three basins north of 30°S, especially in the Pacific Ocean (10.4 Sv) and Indian Ocean (5.0 Sv). The alternating pattern of upwelling and downwelling in the Southern Ocean appears to be topographically controlled (Tamsitt et al. 2018). Net downwelling occurs south of 30°S, with −4.1 Sv in the Atlantic sector, −8.8 Sv in the Pacific sector, and −2.7 Sv in the Indian sector. Comparing the distribution of downwelling in the Southern Ocean sectors with the upwelling in the basin sectors illustrates that substantial exchanges are happening. For example, the −4.1 Sv downwelling in the Atlantic sector exits this sector and upwells in the Indo-Pacific sector (see **Figure 5**). Given the large east–west recirculating transport associated with the ACC (approximately 40 Sv in **Figure 3**, 90 Sv in **Figure 4**, and 20 Sv in **Figure 5**), it is not possible without further analysis to determine the origin of the few sverdrups upwelling and downwelling in each sector.

And it is just as difficult to identify the path of the northward return branch of the mid-depth cell into the Atlantic. **Figure 3** shows that above $\sigma_2 = 37$ kg/m^3, there are 46.0 Sv entering the Atlantic sector of the Southern Ocean through the Drake Passage and 42.7 Sv leaving at 20°E (south of Africa). This 3.3-Sv deficit is due partly to intermediate and thermocline water entering the Atlantic basin from the Pacific Ocean through the Drake Passage (i.e., flowing eastward and

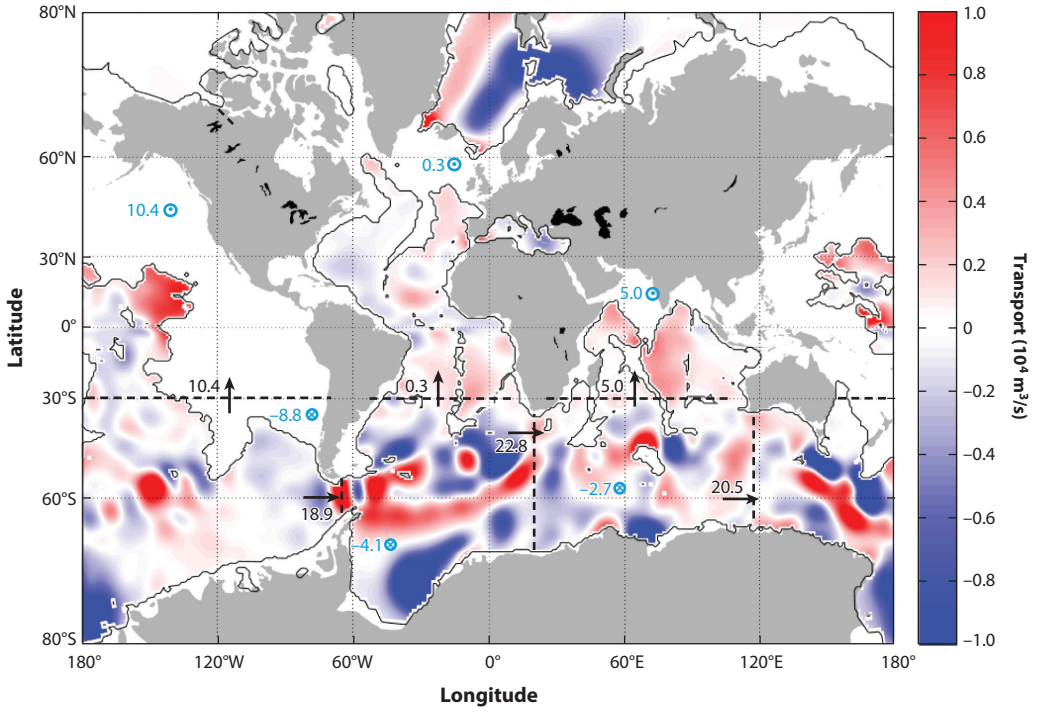

Figure 5

Smoothed diapycnal transport across the $\sigma_2 = 37.52$ kg/m^3 isopycnal (*colors*), showing section transports integrated vertically between the seafloor and $\sigma_2 = 37.52$ kg/m^3 (*black numerals with arrows*). Also shown are the net diapycnal transports horizontally integrated over the six sectors across the $\sigma_2 = 37.52$ kg/m^3 isopycnal (*blue numerals with circles*). The dotted circles indicate upwelling, and the crossed circles indicate downwelling. The black contour shows the climatological intersection at the bottom (incrop) of the $\sigma_2 = 37.52$ kg/m^3 isopycnal.

northward), which is termed the cold route because it transports water that is cold and fresh. A complementary route enters the Atlantic basin from the Indian Ocean, flowing westward and northward around the tip of South Africa, which is termed the warm route because it transports water that is warm and salty. Observational and model estimates attribute different fractions of the transport to each route: Some favor the cold route through the Drake Passage (Rintoul 1991, Sloyan & Rintoul 2001), while others emphasize the warm route south of Africa (Gordon 1986a,b; Speich et al. 2002). The distinction between these two routes is important because it determines the freshwater transport out of the Atlantic basin effected by the AMOC: For the warm route, the AMOC exports fresh water at 30°S, while for the cold route, the AMOC imports fresh water at 30°S. Only in the former case does theoretical and modeling work indicate that the AMOC is potentially bistable, i.e., that there is another equilibrium state with a collapsed AMOC that can be triggered by changes in surface freshwater fluxes in the Labrador and Northern Seas (de Vries & Weber 2005).

In summary, observations agree on the overall transport of the mid-depth cell, both at its maximum and across 30°S. The transport of the abyssal cell is less certain, reflecting inadequate sampling due to its depth and the fact that it is spread over a much larger area. The interbasin and intercell exchanges in the Southern Ocean are obscured by a recirculating circumpolar east–west transport that is at least an order of magnitude larger than the exchanges. In the following sections,

I discuss some recent advances in our understanding of the global overturning circulation, mostly in the context of simplified models.

2. PROCESSES SUSTAINING THE MID-DEPTH CELL

Despite the uncertainties in the detailed pathways of the global overturning circulation, the last decade has seen substantial progress in the understanding of the mechanisms driving the AMOC and, to a lesser extent, the abyssal cell. The mid-depth and abyssal cells are controlled by a combination of local and nonlocal processes. The primary nonlocal process is the wind-driven overturning in the ACC region, i.e., in the subpolar section of the Southern Ocean (Toggweiler & Samuels 1993). In this region, water flows circumpolarly, uninterrupted in longitude, down to the maximum depth of the Drake Passage (2,400 m). This configuration implies that the equatorward Ekman flow of the circumpolar westerlies is returned poleward at depths below 2,400 m, allowing a deep clockwise overturning called the Deacon cell. The Deacon cell carries high-buoyancy water equatorward and low-buoyancy water poleward—i.e., it transports buoyancy equatorward, favoring a convectively unstable state that would result in vertical isopycnals (buoyancy is constant in depth but with horizontal gradients). Such a configuration, however, is optimal for the development of baroclinic eddies that transport buoyancy poleward, partially counteracting the Deacon cell. In the process, baroclinic eddies restratify the water column to a stably stratified state. Despite the baroclinic restratification, the resulting isopycnal slope is steeper in the circumpolar region than it is elsewhere (see **Figure 1**). The goal of this section is to quantify the detailed buoyancy balance controlling the stratification in the ACC region. The net result is that high buoyancy is brought to the mid-depth and abyssal regions by the steep slope of the isopycnals in the ACC region.

The current paradigm is that the mid-depth and abyssal stratification is set in the circumpolar region of the Southern Ocean through a three-term balance between the opposing transports of buoyancy by three distinct processes: the Deacon cell, the eddies, and the meridional overturning. The meridional overturning depends on the mid-depth and abyssal dynamics in the basin portion of the domain, including the highest latitudes, making the balance global. Conceptually, it is useful to first focus on the buoyancy balance in the circumpolar (ACC) region. In this region, it is meaningful to consider the time and zonally averaged buoyancy, $\bar{b}$, the approximate equilibrium of which is given by[2]

$$\bar{v}\partial_y\bar{b} + \bar{w}\partial_z\bar{b} + \partial_y(\overline{v'b'}) + \partial_z(\overline{w'b'}) \approx 0, \qquad 1.$$

where $\bar{v}$ and $\bar{w}$ denote the zonally averaged velocity in the meridional and vertical directions, respectively. This velocity is associated with the surface Ekman transport. With the overbar denoting the time and zonal average, $\overline{v'b'}$ and $\overline{w'b'}$ are the buoyancy fluxes effected by the combination of eddies and standing waves in the latitudinal–vertical (y–z) plane. The balance represented by Equation 1 is not exact because diapycnal mixing has been neglected, which is an acceptable approximation in the circumpolar region below the mixed layer and above the bottom boundary layer. Below the Ekman layer, the horizontal flow is in geostrophic balance, and therefore the zonally averaged meridional and vertical velocities are given respectively by

$$\bar{v} = 0, \quad \bar{w} = -\partial_y\left(\frac{\tau}{\rho f}\right). \qquad 2.$$

It is useful to rewrite Equation 1 in terms of the streamfunctions $\bar{\psi}$ and ψ^* in the latitudinal–vertical (y–z) plane: $\bar{\psi}$ is associated with the mean flow, such that $\partial_y\bar{\psi} = \bar{w}$ and $\partial_z\bar{\psi} = -\bar{v}$, and

[2]The buoyancy is proportional to minus the density multiplied by the gravitational acceleration.

ψ^* is the mean transport per unit width (in square meters per second) associated with eddy fluxes. That is, we define

$$\bar{\psi} \equiv -\frac{\bar{\tau}}{\rho f}, \quad \psi^* \equiv \frac{\overline{v'b'}}{\partial_z \bar{b}}\,, \tag{3.}$$

where τ is the zonal wind stress at the surface, ρ is the ocean density, and f is the Coriolis parameter. Assuming that the eddy fluxes are along mean buoyancy surfaces—eddies do not experience diapycnal mixing—implies

$$\overline{v'b'}\partial_y \bar{b} + \overline{w'b'}\partial_z \bar{b} = 0\,, \tag{4.}$$

so that the buoyancy balance in Equation 1 can be written as

$$\partial_y(\bar{\psi} + \psi^*)\partial_z \bar{b} - \partial_z(\bar{\psi} + \psi^*)\partial_y \bar{b} = 0\,. \tag{5.}$$

In other words, the time and zonally averaged buoyancy is conserved following the residual circulation, $\psi^\dagger \equiv \bar{\psi} + \psi^*$, defined as the sum of Eulerian and eddy transports per unit width. Equivalently, the residual circulation is constant on averaged buoyancy surfaces—i.e., $\psi^\dagger$ is only a function of $\bar{b}$. Although ψ^* is not generally expressible in terms of the mean quantities, the balance represented by Equation 5 is conceptually useful to understand the processes that determine the stratification in the circumpolar region. Simple models of the stratification in the ACC region, assuming zero residual circulation, were given by Marshall & Radko (2003).

In general, the balance between the two opposing processes of Ekman and eddy transport is measured by the residual circulation, $\psi^\dagger$, determined by a diabatic process at the formation sites of deep water, far away from the circumpolar region, and by global diapycnal mixing. Determining the stratification in the ACC region requires examining the dynamics of the overturning in the basins' region. Marshall & Radko (2003) avoided these difficulties by setting $\psi^\dagger = 0$, a simple limit.

3. STRATIFICATION AND RESIDUAL OVERTURNING IN THE QUASI-ADIABATIC LIMIT: THE MID-DEPTH CELL

The approximate adiabatic[3] balance represented by Equation 5 allows a simple theoretical framework for two significant features seen in **Figures 1** and **2**: (*a*) the existence of a mid-depth cell in the Atlantic but not in the Pacific and (*b*) the outcrop of mid-depth isopycnals in the circumpolar region and the North Atlantic but not in the North Pacific.

The stratification and overturning at mid-depth are best understood in the context of a single basin with a circumpolar opening at the southern end of the domain. With reference to **Figure 6**, we can divide the buoyancy surfaces into three regions: (*a*) the thermocline, where isopycnals only outcrop equatorward of the circumpolar portion of the domain; (*b*) the mid-depth region, where isopycnals outcrop in both the circumpolar domain and the high latitudes of the Northern Hemisphere; and (*c*) the abyssal region, where isopycnals outcrop only in the circumpolar region, encountering the solid boundary in the Northern Hemisphere.

In the thermocline, the subtropical cells associated with the Ekman flow are shallow, and surface buoyancy gradients reach only a few hundred meters deep. At mid-depth, northward flow proceeds adiabatically—i.e., without crossing isopycnals—between the high-latitude end points of the mid-depth cell, and it crosses isopycnals only in the surface mixed layer, where there is ample diapycnal mixing. Thus, northward adiabatic flow in the interior can occur only along

[3]The term adiabatic is synonymous with "not subject to diapycnal mixing."

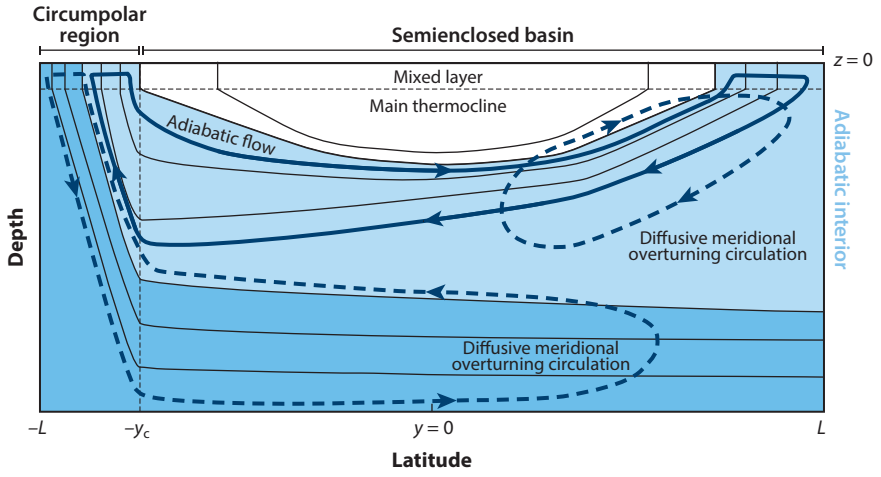

Figure 6

Schematic view of the zonally averaged buoyancy surfaces, showing the three regions: the thermocline, i.e., buoyancy surfaces that do not outcrop in the circumpolar region (*white area*); the mid-depth region, i.e., buoyancy surfaces that outcrop in both the circumpolar region and the Northern Hemisphere (*light blue area*); and the abyssal region, i.e., buoyancy surfaces that outcrop only in the circumpolar region (*dark blue area*).

those isopycnals that outcrop in both the circumpolar region and the Northern Hemisphere. The ensuing interhemispheric cell reaches a depth of approximately 2,500 m, and this depth is set in the circumpolar region, where the isopycnal slope is steep. Isopycnals outcropping in high latitudes of both hemispheres are found in the Atlantic sector but not in the Indo-Pacific sector. To support adiabatic northward flow, there must be surface buoyancy loss at one outcropping end of the cell (i.e., where NADW is formed) and surface buoyancy gain at the opposite outcrop (i.e., in the circumpolar region) in the range of buoyancy characterizing the upper branch of the mid-depth cell—i.e., for 36 kg/m^3 $< \sigma_2 <$ 37 kg/m^3 in **Figure 2*a*** (Wolfe & Cessi 2010, 2011). Indeed, a surface buoyancy gain is observed in the northern part of the circumpolar region (see figure 3 of Ferrari et al. 2014), although there is much uncertainty about the quantitative surface buoyancy flux in the circumpolar region (Lumpkin & Speer 2007, Talley 2013).

With a series of eddy-resolving numerical experiments, Wolfe & Cessi (2010) have illustrated that the Deacon cell in the circumpolar region is essential to establishing deep-reaching stratification and that shared isopycnal outcrops are essential to have an interhemispheric overturning in the limit of weak diapycnal mixing. **Figure 7** shows the time and zonally averaged isotherms for two computations forced by surface wind stress and a prescribed surface temperature in two different geometries (isotherms coincide with isopycnals in this case). The case without a circumpolar, periodic opening in the south is unstratified below the wind-driven subtropical thermocline (**Figure 7**). The circumpolar opening is essential in order to push the buoyancy gradients down to the mid-depth and abyssal regions, because north–south boundaries allow an east–west pressure difference associated with a geostrophic flow that returns the surface Ekman transport at shallow depths (**Figure 7*b***).

Figure 8 shows the time and zonally averaged residual overturning circulation for two computations with the same domain but different prescribed surface temperatures. When the surface temperature is such that there are no surface isopycnals shared between the circumpolar region and the Northern Hemisphere (the warm-pole case shown in **Figure 8*c***), the mid-depth cell is weak (**Figure 8*a***); when there are shared surface isopycnals between the circumpolar region and

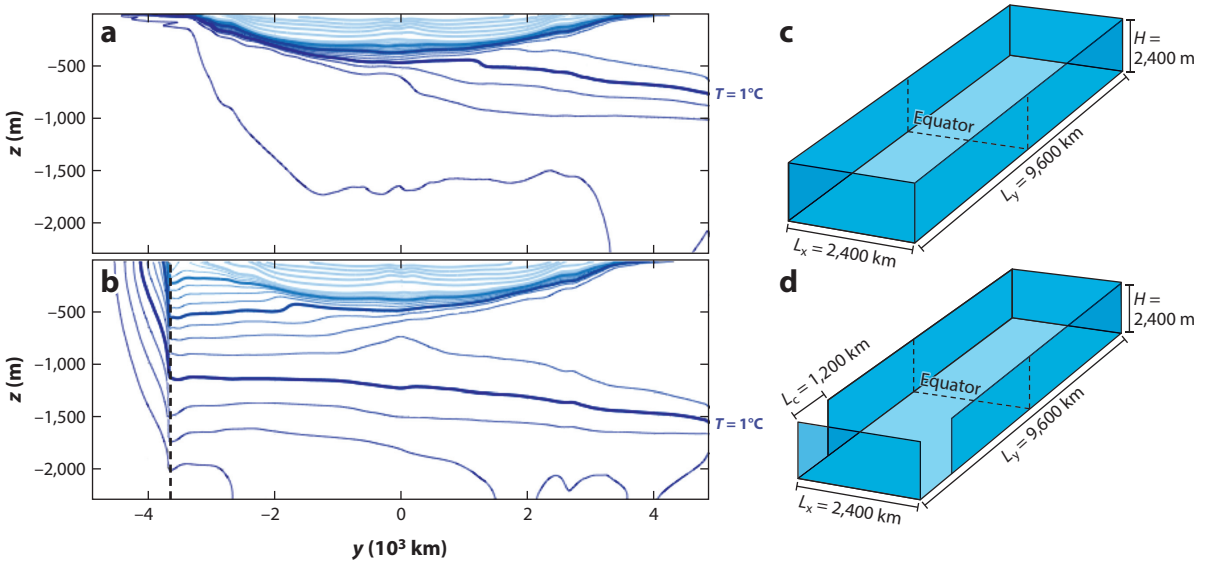

Figure 7

Time and zonally averaged temperature as a function of latitude and depth (panels *a* and *b*) for two experiments differing only in their geometry (panels *c* and *d*). The thickest blue line in panels *a* and *b* is $T = 1°C$, and the contour interval is 0.5°C for $T \leq 4°C$ and 2°C for $T > 4°C$. Without the periodic opening at the southern edge of the domain (panel *b*), the mid-depth and abyssal regions are unstratified, and all the buoyancy gradients are confined to the thermocline.

the Northern Hemisphere (the cold-pole case shown in **Figure 8*c***), the mid-depth cell is strong (**Figure 8*b***). The stratification is not shown in the figure, but it is qualitatively similar in both cases. For a completely closed domain (no circumpolar region), the residual overturning is qualitatively similar to the warm-pole case (**Figure 8*a***).

Nikurashin & Vallis (2012) developed a simplified theory of the mid-depth cell that incorporates the conceptual framework of Wolfe & Cessi (2010). The theory expresses the time and zonally averaged eddy transports, $\overline{v'b'}$ and $\overline{w'b'}$, in terms of the time and zonally averaged buoyancy, $\bar{b}$, using the well-established Gent–McWilliams parameterization (Gent & McWilliams 1990, Griffies 1998). With this parameterization, the eddy streamfunction, ψ^*, is expressed as $\psi^* = -K\partial_y\bar{b}/\partial_z\bar{b}$, i.e., proportional to the slope of the isopycnals. Thus, in the circumpolar region, where Equation 1 holds, the slope of the isopycnals is given by

$$-\frac{\partial_y\bar{b}}{\partial_z\bar{b}} = K^{-1}\left[\psi^\dagger(\bar{b}) + \frac{\bar{\tau}(y)}{\rho f}\right]. \qquad 6.$$

With this parameterization, once K is prescribed, Equation 6 predicts the slope of the isopycnals in the circumpolar region given the surface wind stress and the residual overturning. The latter is determined by matching the overturning cell at the boundary between the circumpolar region and the basin. Note that in the circumpolar region, the second term on the right side of Equation 6 is negative (westerly winds and $f < 0$ in the Southern Hemisphere). The residual overturning is positive for the mid-depth cell and negative for the abyssal cell, reducing the mid-depth negative slopes of the isopycnals in the circumpolar region and increasing the abyssal isopycnal slopes. In the limit of negligible diapycnal mixing in the basin interior, $\psi^\dagger(\bar{b})$ is determined at the southern edge of the deep-water (NADW) formation region and preserved along the isopycnals all the way to the edge of the circumpolar region (Nikurashin & Vallis 2012). Diapycnal mixing can

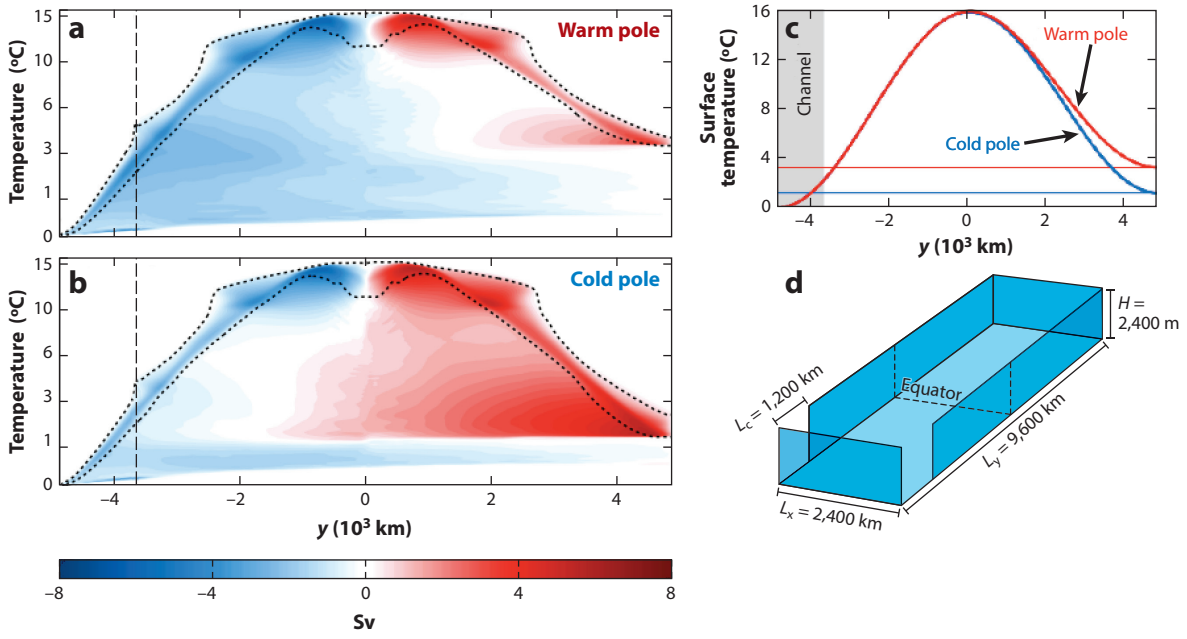

Figure 8

Time and zonally averaged residual overturning circulation as a function of latitude and temperature (panels *a* and *b*) for two experiments differing only in the prescribed surface temperatures shown in panel *c*. Both experiments have the geometry shown in panel *d*. The vertical dashed line denotes the latitude of the northern edge of the periodic (Antarctic Circumpolar Current) region. In panel *b*, there is no buoyancy surfacing in both the circumpolar and Northern Hemisphere regions, and the interhemispheric mid-depth cell (*red contours*) is very weak. The stratification (not shown) is similar in both cases.

quantitatively modify $\psi^\dagger$, and the resulting scaling, given by Nikurashin & Vallis (2012), was anticipated by Gnanadesikan (1999), given by the solution, h, of the buoyancy balance at the edge of the circumpolar region, i.e.,

$$-K\frac{h}{l} = \frac{\Delta b h^2}{f_n L_x} - \frac{\kappa_v L}{h} + \frac{\bar{\tau}}{\rho f_s}. \qquad 7.$$

Equation 7 represents the same balance as Equation 6, except that it is given in terms of scales rather than local values and explicitly expresses $\psi^\dagger$ at the boundary between the circumpolar and basin regions with the first two terms on the right side. The unknown in Equation 7 is the depth reached by the mid-depth stratification at the poleward edge of the circumpolar region, h (h/l is the associated isopycnal slope, with l the latitudinal extent of the circumpolar region). The residual overturning at the southern edge of the basin, $\psi^\dagger$, has two contributions. The first term on the right side of Equation 7 expresses the geostrophic transport per unit longitude out of the Northern Hemisphere convective region, which is characterized by the range of surface isopycnals shared with the circumpolar region, Δb; the Coriolis parameter, f_n (positive); and the longitudinal extent of the basin, L_x. The second term on the right side of Equation 7 is the diffusive contribution, which is proportional to the latitudinal extent of the basin, L, and the diapycnal diffusivity, κ_v. The last term on the right side of Equation 7 is minus the Ekman transport at the northern edge of the circumpolar region (negative because of the Coriolis parameter, f_s). The solution of Equation 7 shows that the depth reached by the intermediate stratification, h, and the amplitude of the overturning both increase with the westerly wind stress in the ACC region and the strength of

diapycnal mixing and decrease with the strength of the buoyancy transport by mesoscale eddies in the circumpolar region. From Equation 7, it is clear that in the limit of weak eddy transport ($K \to 0$) and weak diapycnal mixing ($\kappa_v \to 0$), the residual overturning is equal to the Ekman transport at the northern edge of the circumpolar region, and the stratification penetrates to a depth, h, proportional to the square root of the wind stress in the circumpolar region and inversely proportional to the square root of the range of shared isopycnals (Gnanadesikan 1999). The similarity with Welander's scaling for the depth of the upper-ocean thermocline is only superficial because Equation 7 relates quantities in opposite hemispheres, while for the Welander thermocline all quantities are local. In the limit of large diapycnal mixing, the first and second terms on the right-hand side balance, recovering the classic local diffusive scaling where $h \sim \kappa_v^{1/3}$ and $\psi^\dagger \sim \kappa_v^{2/3}$ (Welander 1971).

4. STRATIFICATION AND RESIDUAL OVERTURNING IN THE DIFFUSIVE REGIME: THE ABYSSAL CELL

While there is a good theoretical understanding of the quasi-adiabatic dynamics of the intermediate circulation associated with the AMOC, the detailed dynamics of the abyssal cell are less developed. The negative buoyancy flux entering the cell at the surface near the Antarctic margin must be balanced by positive diapycnal diffusion in the interior of the cell, i.e., diapycnal upwelling. While it is clear that the strength of the abyssal cell is proportional to the diapycnal diffusivity, the precise power law and dependence on the other parameters of the problem, such as the wind stress and surface buoyancy flux, have not been firmly established. Efforts to connect the stratification and circulation in the circumpolar region to the abyssal region have been led by Ito & Marshall (2008), Nikurashin & Vallis (2011), Mashayek et al. (2015), and Jansen & Nadeau (2016). The common framework of these works is that the abyssal stratification in the circumpolar region obeys similar dynamics as the mid-depth levels, where the residual overturning, $\psi^\dagger$, is given by the balance between the Ekman-flow overturning, $\bar{\psi}$, and the restratification by eddy (and standing-wave) buoyancy fluxes, represented by ψ^*. As in the treatment of the mid-depth circulation, diapycnal mixing is neglected in the circumpolar region, away from the top mixed layer and the bottom boundary layer, and the residual overturning, $\psi^\dagger$, is determined by matching the circumpolar dynamics to the basin dynamics at the common latitudinal boundary. The main difference with the mid-depth cell is that there is no water-mass formation in the Northern Hemisphere part of the basin, and diapycnal mixing is certainly important.

The simplest way to understand the abyssal dynamics is to again use the scaling formulation given in Equation 7, appropriately modified to suit the abyssal balance. For example, Ito & Marshall (2008) and Nikurashin & Vallis (2011) assumed that the abyssal cell extends all the way to the northern boundary of the basin, so its latitudinal extent, L, is known and coincides with the basin length. In the absence of Northern Hemisphere abyssal water formation, they found the balance

$$-K\frac{h}{l} = -\frac{\kappa_v L}{h} + \frac{\bar{\tau}}{\rho f_s}. \qquad 8.$$

For large diffusivity, the wind-stress term is negligible and there is a balance between the eddy-induced slope in the circumpolar region and diapycnal mixing in the basin, so that $h = \sqrt{(\kappa_v L l / K)}$.

Mashayek et al. (2015) added another physical process by considering the diapycnal mixing to increase toward the ocean bottom, as observed. In addition, they allowed L to be an unknown, dynamically determined meridional scale—i.e., the abyssal cell does not extend all the way to the northern edge of the basin, consistent with the observations (see **Figures 2*b*** and **5**). Mashayek et al. (2015) also neglected the wind-stress component relative to the eddy component, because

the abyssal isopycnal slopes are quite steep, to arrive at the balance

$$-K\frac{b}{l} = -\frac{\kappa_v L}{b} + \frac{\kappa_v L}{H_{\mathrm{mix}}}. \qquad 9.$$

The second term on the right side of Equation 9 represents the contribution due to the variation of the diapycnal mixing with depth, on the given scale H_{mix}. There are two possible balances in Equation 9. First, the eddy-induced slope balances the diapycnal mixing (the left side balances the first term on the right side of Equation 9); this scaling applies in the bottom part of the abyssal cell and is equivalent to the scaling of Nikurashin & Vallis (2011), except that L is smaller than the total basin length and is unknown. Alternatively, the vertical scale of the isopycnals, b, coincides with H_{mix}; this scaling applies to the transition region between the mid-depth and abyssal cells, where the diapycnal mixing changes rapidly. Surprisingly, none of the scalings presented so far depend on the surface buoyancy flux. Jansen & Nadeau (2016) have studied the response of the abyssal cell to changes in the surface buoyancy flux, also in the context of a single basin. They found that, in a single basin, there is competition between the mid-depth and abyssal cells, so the scaling in Equation 9 applies only when the two cells are well separated in the vertical.

The scaling and theories summarized above assume constant ocean depth. A growing body of literature is showing the important effects on the abyssal stratification and circulation due to the interaction of sloping boundaries with bottom-enhanced mixing (Polzin et al. 1997, de Lavergne et al. 2016b, Ferrari et al. 2016, McDougall & Ferrari 2017, Holmes et al. 2018). First, the increase of energy dissipation with depth implies a corresponding increase of diapycnal buoyancy flux. This increase is reversed in a thin bottom boundary layer, which brings said flux to zero (or to the geothermal buoyancy flux). In turn, the increase in diapycnal buoyancy flux with depth is associated with diapycnal downwelling, i.e., a circulation that is opposite to that required to balance the production of bottom water. To see this, it is useful to consider the diapycnal velocity, approximated with the vertical velocity, w (positive upward), to satisfy the abyssal balance given by

$$w \approx \frac{1}{\partial_z b}\partial_z\left(\kappa_v \partial_z b\right) = \frac{1}{\partial_z b}\partial_z\left(\Gamma\varepsilon\right), \qquad 10.$$

where ε is the turbulent energy dissipation and Γ is the mixing efficiency. The observed oceanic range of Γ is 0.1–0.3 (Gregg et al. 2018), while the turbulent energy dissipation increases with depth by two orders of magnitude near rough topography, so the diffusive flux $-\Gamma\varepsilon$ becomes more negative with depth. Because of stable stratification, $\partial_z b > 0$, Equation 10 implies $w < 0$, i.e., downwelling (de Lavergne et al. 2016a,b; Ferrari et al. 2016). Overall, the closure of the abyssal cell requires upwelling in the abyssal interior. Upwelling is possible with sloping topography in the bottom boundary layer, because this is the layer where the buoyancy flux goes from large negative values to zero at the solid boundary (or positive in regions of active geothermal heating). Using arguments based on laminar dynamics, McDougall & Ferrari (2017) and Holmes et al. (2018) indicated that the nature of the boundary-layer upwelling is strongly controlled by the details of the topography, i.e., its slope, curvature, and bathymetric contour length. To be clear, these geometrical properties are fractal. But the quantities relevant for boundary-layer upwelling are smoothed over the depth of the stratified layer where there is enhanced mixing (i.e., a few hundred meters above the rough bottom) and over a horizontal length that depends on the slope on this vertical scale (i.e., a few hundred kilometers).

Although these theories have not yet delivered explicit scaling laws, results from numerical simulations implementing bottom-enhanced diffusivities near sloping boundaries show that the abyssal circulation and stratification are substantially increased compared with small uniform

diffusivity, while the mid-depth circulation and stratification are essentially unaffected (Saenko & Merryfield 2005, Jayne 2009, Melet et al. 2016).

5. GLOBAL STRATIFICATION AND OVERTURNING

The theories summarized in the previous sections consider a single overturning basin, ignoring the fundamental asymmetry between the Atlantic, which has an interhemispheric mid-depth cell, and the Indo-Pacific, which has no mid-depth cell but does have an abyssal cell. Because the Indo-Pacific sector lacks any isopycnal that outcrops simultaneously in the circumpolar region and in the high latitudes of the Northern Hemisphere, it is not possible to establish the adiabatic flow that characterizes the interior part of the mid-depth cell, and only the diffusive abyssal cell is possible.

The main reason why the isopycnals outcropping in the circumpolar region do not surface in the North Pacific is that its sea-surface salinity is lower than that of the North Atlantic. This salinity asymmetry is caused by both atmospheric processes and intrinsic oceanic mechanisms contributing in approximately equal proportions, as summarized by Ferreira et al. (2018). Atmospheric processes cause the Atlantic (north of 30°S) to evaporate 0.5 Sv (see the blue numbers in **Figure 3**), while the Pacific (north of 30°S) has zero net freshwater flux (see the blue numbers in **Figure 3** and Craig et al. 2017). This difference is the result of two main mechanisms: (*a*) Evaporation caused by midlatitude storms encountering warm oceanic western boundary currents gives more evaporation per unit area in narrow basins, i.e., in the Atlantic (Schmitt et al. 1989), and there is a fetch of approximately 3,000 km between the locations of evaporation (near the coast) and of precipitation, leading to more midlatitude precipitation in wider basins, i.e., the Pacific (Ferreira et al. 2010), and (*b*) there is a net convergence of tropical moisture that is larger in the Pacific than in the Atlantic, primarily because of the flow associated with the Asian monsoon (Emile-Geay et al. 2003). Two main oceanic processes also contribute to higher surface salinity in the Atlantic than in the Pacific: (*a*) The mid-depth cell itself advects salt-rich subtropical waters in the subpolar region, sustaining the overturning, a process called the salt–advection feedback (Stommel 1961, Rooth 1982, Rahmstorf 1996, Wolfe & Cessi 2014), and (*b*) the existence of a short continent (Africa) to the east of the Atlantic basin promotes import of salty subtropical water from the Indian Ocean in the upper levels of the Atlantic, increasing its salinity (Reid 1961; Gordon 1986a,b; Nilsson et al. 2013; Cessi & Jones 2017).

The processes responsible for the creation of intermediate waters in the Atlantic sector—Ekman flow entering at the shallow levels in the circumpolar region and diffuse diapycnal upwelling—also operate in the Indo-Pacific sector. Given that there is no production of deep water in the northern part of the Indo-Pacific sector, the water entering this sector at intermediate levels must exit at the same levels along the southern boundary of the Indo-Pacific, where it is exchanged with the Atlantic through the Southern Ocean. This southward flow is associated with a geostrophically balanced difference in pressure between the Atlantic and Indo-Pacific sectors. Because of hydrostatic balance, this pressure difference is accompanied by deeper isopycnals at the southern edge of the Indo-Pacific relative to the Atlantic, a difference that is then propagated northward throughout the basins (compare the depths of the $\sigma_2 = 37$ surfaces in the two panels of **Figure 1**). This simple property has been demonstrated by Allison (2009) and Jones & Cessi (2016) using an extension of Gnanadesikan's (1999) model to two basins (the Atlantic and the Indo-Pacific) connected by a circumpolar Southern Ocean, and by primitive-equation computations in an ocean model with simplified geometry (Jones & Cessi 2016).

As discussed in Section 1, there are two possible routes for the intermediate waters to move from the Indo-Pacific to the Atlantic—through the Drake Passage (the cold route) and around the

tip of Africa (the warm route)—and analyses of observations disagree on which route carries the most water. On the theoretical side, the conceptual model of Cessi & Jones (2017) predicts that, if the tip of South Africa is north of the boundary between the Southern Hemisphere subtropical and subpolar gyres and the tip of South America is to its south (as is the case in the present climate), then all the intermediate-water transfer from the Indo-Pacific to the Atlantic will go through the warm route. This prediction is supported by primitive-equation computations of an ocean model in simplified geometries of two basins connected by a circumpolar region (Nilsson et al. 2013, Cessi & Jones 2017).

6. THE CONNECTION BETWEEN THE MID-DEPTH AND ABYSSAL CELLS

As discussed in Section 1, the degree of connection between the lower branch of the AMOC and the Indo-Pacific abyssal cell is difficult to constrain quantitatively with observations.

On the theoretical side, Thompson et al. (2016) formulated an eight-box model to explore the two scenarios of NADW upwelling: (*a*) diabatic, via conversion into AABW and upwelling in the abyssal cell in the Indo-Pacific, and (*b*) quasi-adiabatic, via direct upwelling and conversion into intermediate water in the surface mixed layer. They found that the controlling parameter is the ratio of NADW production rate to the mid-depth diapycnal diffusivity: As this ratio increases, the flow becomes more adiabatic, and the return path of NADW becomes disconnected from the abyssal circulation.

Ferrari et al. (2017) designed a series of computations to explore the connection between the mid-depth cell in the Atlantic and the abyssal cell in the Indo-Pacific. Using a simplified geometry of the world ocean, with two basins of unequal width and extent connected by a circumpolar region in the high latitudes of the Southern Hemisphere, forced by surface wind stress and prescribed buoyancy, they explored the connection between the two cells by varying the diapycnal mixing and the details of the high-latitude buoyancy forcing. An interesting interbasin regime is found where deep water is formed in the model North Atlantic, flows quasi-adiabatically to the Southern Ocean, and upwells diabatically in the Indo-Pacific, from deep (not abyssal) to intermediate levels. In addition, a small fraction of deep water is recycled through the abyss. Because the transport of the mid-depth cell in the Atlantic is larger than the transport in the Indo-Pacific, some deep water must be converted quasi-adiabatically. The abyssal recycling of NADW described by Talley (2013) requires the abyssal cell to be stronger than the mid-depth cell, and this regime is not captured in any of the computations presented by Ferrari et al. (2017). It is not clear what the missing ingredient is that would allow the abyssal cell to be stronger than the mid-depth cell.

7. DISCUSSION AND OPEN QUESTIONS

The last decade has seen a shift in conceptual models of the mid-depth overturning circulation and stratification; in these new models, the energy needed to push high-buoyancy water downward to create mid-depth stratification and overturning comes mainly from the wind stress in the circumpolar region, rather than from diapycnal mixing, as originally suggested by Munk (1966). This wind stress drives a Deacon cell and baroclinic eddies that respectively force and drain the mid-depth stratification and circulation. The mid-depth cell exists in the region occupied by buoyancy surfaces that outcrop both in the circumpolar region of the Southern Ocean and in the high latitudes of the Northern Hemisphere. This region allows interhemispheric adiabatic flow of intermediate and thermocline water that connects a region of surface buoyancy loss in the

Northern Hemisphere to one of surface buoyancy gain in the circumpolar region. The mid-depth cell crosses buoyancy surfaces in the surface mixed layer only at the end points of the cell and is not especially affected by interior diapycnal mixing. The adiabaticity of the mid-depth cell is most clearly visualized by the residual streamfunction in the buoyancy coordinates (potential density referenced to 2,100 dbar) shown in **Figure 2*a***.

Erratum >

The quasi-adiabatic, wind-driven dynamics of the mid-depth cell are consistent with the localization of the cell to the Atlantic sector, which has surface buoyancy values at its northern end that are also found in the circumpolar region. Because this isopycnal sharing is not found in the Pacific sector, a corresponding mid-depth cell cannot be supported. Nevertheless, some intermediate water enters the mid-depth region of the Southern Ocean in the Indo-Pacific, and it must be transferred to the Atlantic in order to sink. The precise path of this intermediate-water transfer has not been agreed upon in the literature, despite the relative abundance of data above 1,500 m. The uncertainty arises because the net transfer amounts to a few sverdrups, an order of magnitude smaller than the east–west recirculating circumpolar transport.

The abyssal circulation is powered by diapycnal diffusion, which is enhanced toward the bottom and is more prominent in the Indo-Pacific than in the Atlantic, mainly because of its larger area, especially in the Southern Hemisphere. The negative buoyancy flux entering through the surface at the Antarctic margin must be balanced by a positive diapycnal buoyancy flux (diapycnal upwelling). The diagnostic and theoretical work reported in Section 4 indicates that abyssal upwelling occurs along bottom boundary layers over rough topography, the properties of which are modulated by the slope and arc length of the rough topography (smoothed over appropriate scales), while the abyssal interior experiences diapycnal downwelling. Because of the large cancellation between the interior downwelling and the boundary-layer upwelling, the net upwelling is a small residual, and other processes appear to be as important as locally enhanced energy dissipation (and the associated diapycnal diffusion), including the contribution of geothermal heating and remote dissipation of internal tides. Using a suite of plausible scenarios of spatially varying diapycnal diffusion, de Lavergne et al. (2016b) were able to balance rates of abyssal overturning of 10–15 Sv—rather smaller than those obtained through estimates of the transport (Lumpkin & Speer 2007, Talley 2013) and closer to the transport obtained with the ECCO4 estimate (see **Figure 2**). This discrepancy arises because the abyss is poorly constrained by data in terms of both direct transport measurements and diapycnal buoyancy flux estimates.

The strength of the abyssal cell is correlated with the transformation of NADW into AABW; in the estimates with the larger abyssal cell strength, this contribution is substantial. The few computations that have addressed this question systematically indicate that when the NADW transport is larger than or equal to the AABW transport, there is little conversion of NADW into AABW and little recycling of NADW through the abyssal cell (Thompson et al. 2016, Ferrari et al. 2017).

In summary, the upper branch of the mid-depth cell is fed by a global overturning circulation that involves exchanges with the Indo-Pacific basins as well as the Southern Ocean, but the details of this exchange have not been completely agreed upon in the literature. The degree of connection between the lower branch of the mid-depth overturning and the abyssal cell is even less clear, and a more robust quantification requires better observations of the abyss.

DISCLOSURE STATEMENT

The author is not aware of any affiliations, memberships, funding, or financial holdings that might be perceived as affecting the objectivity of this review.

ACKNOWLEDGMENTS

Support by the National Science Foundation under grants OCE-1258887 and OCE-1634128 is gratefully acknowledged. Many thanks to Xinfeng Liang and Gael Forget for help with the ECCO4 analysis. I benefited from discussions with Joern Callies, C. Spencer Jones, Dorotea Iovino, Malte Jansen, Louis-Philippe Nadeau, Andrea Storto, and Amy Waterhouse. Part of the work on this review was carried out while visiting the Consiglio Nazionale delle Ricerche (CNR) Institute of Atmospheric Sciences and Climate (ISAC) and the Euro-Mediterranean Center on Climate Change (CMCC), whose hospitality is gratefully acknowledged.

LITERATURE CITED

Allison LC. 2009. *Spin-up and adjustment of the Antarctic Circumpolar Current and global pycnocline*. PhD Thesis, Univ. Reading, Reading, UK

Andrews DG, Holton JR, Leovy CB. 1987. *Middle Atmosphere Dynamics*. San Diego, CA; Academic

Bouffard D, Boegman L. 2013. A diapycnal diffusivity model for stratified environmental flows. *Dyn. Atmos. Oceans* 61:14–34

Cessi P, Jones CS. 2017. Warm-route versus cold-route interbasin exchange in the meridional overturning circulation. *J. Phys. Oceanogr.* 47:1981–97

Craig PM, Ferreira D, Methven J. 2017. The contrast between Atlantic and Pacific surface water fluxes. *Tellus A* 69:1330454

de Lavergne C, Madec G, Sommer JL, Nurser A, Garabato AN. 2016a. The impact of a variable mixing efficiency on the abyssal overturning. *J. Phys. Oceanogr.* 46:663–81

de Lavergne C, Madec G, Sommer JL, Nurser A, Garabato AN. 2016b. On the consumption of Antarctic Bottom Water in the abyssal ocean. *J. Phys. Oceanogr.* 46:635–61

de Vries P, Weber SL. 2005. The Atlantic freshwater budget as a diagnostic for the existence of a stable shut down of the meridional overturning circulation. *Geophys. Res. Lett.* 32:L09606

Emile-Geay J, Cane MA, Naik N, Seager R, Clement AC, van Green A. 2003. Warren revisited: atmospheric freshwater fluxes and "Why is no deep water formed in the North Pacific." *J. Geophys. Res.* 108:3178

Ferrari R, Jansen MF, Adkins JF, Burke A, Stewart AL, Thompson AF. 2014. Antarctic sea ice control on ocean circulation in present and glacial climates. *PNAS* 111:8753–58

Ferrari R, Mashayek A, McDougall T, Nikurashin M, Campin-Michael JM. 2016. Turning ocean mixing upside down. *J. Phys. Oceanogr.* 46:2239–61

Ferrari R, Nadeau LP, Marshall DP, Allison LC, Johnson HL. 2017. A model of the ocean overturning circulation with two closed basins and a reentrant channel. *J. Phys. Oceanogr.* 47:2887–906

Ferreira D, Cessi P, Coxall H, de Boer A, Dijkstra H, et al. 2018. Atlantic-Pacific asymmetry in deep water formation. *Annu. Rev. Earth Planet. Sci.* 46:327–52

Ferreira D, Marshall J, Campin JM. 2010. Localization of deep water formation: role of atmospheric moisture transport and geometrical constraints on ocean circulation. *J. Clim.* 23:1456–76

Forget G, Campin JM, Heimbach P, Hill CN, Ponte RM, Wunsch C. 2015. ECCO version 4: a global ocean modeling and state estimation framework. *Geosci. Model Dev.* 8:3071–104

Gent PR, McWilliams JC. 1990. Isopycnal mixing in ocean circulation models. *J. Phys. Oceanogr.* 20:150–55

Gnanadesikan A. 1999. A simple predictive model for the structure of the oceanic pycnocline. *Science* 283:2077–79

Gordon AL. 1986a. Interocean exchange of thermocline water. *J. Geophys. Res.* 91:5037–46

Gordon AL. 1986b. Is there a global scale ocean circulation? *Eos Trans. AGU* 67:109–10

Gregg MC, D'Asaro EA, Riley JJ, Kunze E. 2018. Mixing efficiency in the ocean. *Annu. Rev. Mar. Sci.* 10:443–73

Griffies SM. 1998. The Gent–McWilliams skew flux. *J. Phys. Oceanogr.* 28:831–41

Henyey FS, Wright J, Flatté SM. 1986. Energy and action flow through the internal wave field: an eikonal approach. *J. Geophys. Res.* 91:8487–95

Holmes RM, de Lavergne C, McDougall T. 2018. Ridges, seamounts, troughs and bowls: topographic control of the dianeutral circulation in the abyssal ocean. *J. Phys. Oceanogr.* 48:861–82

Ito T, Marshall J. 2008. Control of lower-limb overturning circulation in the Southern Ocean by diapycnal mixing and mesoscale eddy transfer. *J. Phys. Oceanogr.* 38:2832–45

Jansen MF, Nadeau LP. 2016. The effect of Southern Ocean surface buoyancy loss on the deep-ocean circulation and stratification. *J. Phys. Oceanogr.* 46:3455–70

Jayne SR. 2009. The impact of abyssal mixing parameterizations in an ocean general circulation model. *J. Phys. Oceanogr.* 39:1756–75

Jones CS, Cessi P. 2016. Interbasin transport of the meridional overturning circulation. *J. Phys. Oceanogr.* 46:1157–69

Kuhlbrodt T, Griesel A, Montoya M, Levermann A, Hofmann M, Rahmstorf S. 2007. On the driving processes of the Atlantic meridional overturning circulation. *Rev. Geophys.* 45:RG2001

Kunze E. 2017. The internal-wave-driven meridional overturning circulation. *J. Phys. Oceanogr.* 47:2673–89

Kunze E, Firing E, Hummon JM, Chereskin TK, Thurnherr AM. 2006. Global abyssal mixing inferred from lowered ADCP shear and CTD strain profiles. *J. Phys. Oceanogr.* 36:1553–76

Lumpkin R, Speer K. 2007. Global ocean meridional overturning. *J. Phys. Oceanogr.* 37:2550–62

Marshall J, Radko T. 2003. Residual-mean solutions for the Antarctic Circumpolar Current and its associated overturning circulation. *J. Phys. Oceanogr.* 33:2341–54

Marshall J, Speer K. 2012. Closure of the meridional overturning circulation through Southern Ocean upwelling. *Nat. Geosci.* 5:171–80

Mashayek A, Ferrari R, Nikurashin M, Peltier W. 2015. Influence of enhanced abyssal diapycnal mixing on stratification and the ocean overturning circulation. *J. Phys. Oceanogr.* 45:2580–97

McCarthy GD, Smeed DA, Johns WE, Frajka-Williams E, Moat BI, et al. 2015. Measuring the Atlantic meridional overturning circulation at 26°N. *Prog. Oceanogr.* 130:91–111

McDougall TJ, Ferrari R. 2017. Abyssal upwelling and downwelling driven by near-boundary mixing. *J. Phys. Oceanogr.* 47:261–83

Meinen CS, Speich S, Piola AR, Ansorge I, Campos E, et al. 2018. Meridional overturning circulation transport variability at 34.5°S during 2009–2017: baroclinic and barotropic flows and the dueling influence of the boundaries. *Geophys. Res. Lett.* 45:4810–88

Melet A, Legg S, Hallberg R. 2016. Climatic impacts of parameterized local and remote tidal mixing. *J. Clim.* 29:3473–500

Munk WH. 1966. Abyssal recipes. *Deep-Sea Res. Oceanogr. Abstr.* 13:707–30

Nikurashin M, Ferrari R. 2013. Overturning circulation driven by breaking internal waves in the deep ocean. *Geophys. Res. Lett.* 40:3133–37

Nikurashin M, Vallis G. 2011. A theory of deep stratification and overturning circulation in the ocean. *J. Phys. Oceanogr.* 41:485–502

Nikurashin M, Vallis G. 2012. A theory of the interhemispheric meridional overturning circulation and associated stratification. *J. Phys. Oceanogr.* 42:1652–67

Nilsson J, Langen PL, Ferreira D, Marshall J. 2013. Ocean basin geometry and the salinification of the Atlantic Ocean. *J. Clim.* 26:6163–84

Polzin KL, Toole JM, Ledwell JR, Schmitt RW. 1997. Spatial variability of turbulent mixing in the abyssal ocean. *Science* 276:93–96

Rahmstorf S. 1996. On the freshwater forcing and transport of the Atlantic thermohaline circulation. *Clim. Dyn.* 12:799–811

Reid JL. 1961. On the temperature, salinity, and density differences between the Atlantic and Pacific oceans in the upper kilometre. *Deep-Sea Res.* 7:265–75

Ridgway KR, Dunn JR. 2007. Observational evidence for a Southern Hemisphere oceanic supergyre. *Geophys. Res. Lett.* 34:L13612

Rintoul SR. 1991. South Atlantic interbasin exchange. *J. Geophys. Res.* 96:2675–92

Rooth C. 1982. Hydrology and ocean circulation. *Prog. Oceanogr.* 11:131–49

Saenko O, Merryfield W. 2005. On the effect of topographically enhanced mixing on the global ocean circulation. *J. Phys. Oceanogr.* 35:826–34

Schmitt RW, Bogden PS, Dorman CE. 1989. Evaporation minus precipitation and density fluxes for the North Atlantic. *J. Phys. Oceanogr.* 19:1208–21

Sloyan BM, Rintoul SR. 2001. Circulation, renewal, and modification of Antarctic Mode and Intermediate Water. *J. Phys. Oceanogr.* 31:1005–30
Speich S, Blanke B, Cai W. 2007. Atlantic meridional overturning circulation and the Southern Hemisphere supergyre. *Geophys. Res. Lett.* 34:L23614
Speich S, Blanke B, de Vries P, Drijfhout S, Döös K, et al. 2002. Tasman leakage: a new route in the global ocean conveyor belt. *Geophys. Res. Lett.* 29:55-1–4
St. Laurent LC, Simmons HL, Jayne SR. 2002. Estimating tidally driven mixing in the deep ocean. *Geophys. Res. Lett.* 29:21-1–4
Stommel H. 1961. Thermohaline convection with two stable regimes of flow. *Tellus* 13:224–30
Talley LD. 2013. Closure of the global overturning circulation through the Indian, Pacific, and Southern Oceans: schematics and transports. *Oceanography* 26(1):80–97
Tamsitt V, Abernathey RP, Mazloff MR, Wang J, Talley LD. 2018. Transformation of deep water masses along Lagrangian upwelling pathways in the Southern Ocean. *J. Geophys. Res. Oceans* 123:1994–2017
Thompson AF, Stewart A, Bischoff T. 2016. A multibasin residual-mean model for the global overturning circulation. *J. Phys. Oceanogr.* 46:2583–604
Toggweiler JR, Samuels B. 1993. New radiocarbon constraints on the upwelling of abyssal water to the ocean's surface. In *The Global Carbon Cycle*, ed. M Heimann, pp. 333–66. New York: Springer
Waterhouse AF, MacKinnon JA, Nash JD, Alford MH, Kunze E, et al. 2014. Global patterns of diapycnal mixing from measurements of the turbulent dissipation rate. *J. Phys. Oceanogr.* 44:1854–72
Welander P. 1971. The thermocline problem. *Philos. Trans. R. Soc. Lond. A* 270:69–73
Whalen CB, MacKinnon JA, Talley LD, Waterhouse AF. 2015. Estimating the mean diapycnal mixing using a finescale strain parameterization. *J. Phys. Oceanogr.* 45:1174–88
Wolfe CL, Cessi P. 2010. What sets the strength of the mid-depth stratification and overturning circulation in eddying ocean models? *J. Phys. Oceanogr.* 40:1520–38
Wolfe CL, Cessi P. 2011. The adiabatic pole-to-pole overturning circulation. *J. Phys. Oceanogr.* 41:1795–810
Wolfe CL, Cessi P. 2014. Salt feedback in the adiabatic overturning circulation. *J. Phys. Oceanogr.* 44:1175–94
Young WR. 2012. An exact thickness-weighted average formulation of the Boussinesq equations. *J. Phys. Oceanogr.* 42:692–707

Annual Review
of Marine Science

Volume 11, 2019

Contents

Errata

An online log of corrections to *Annual Review of Marine Science* articles may be found at http://www.annualreviews.org/errata/marine